doi:10.1016/j.jmb.2011.07.015 J. Mol. Biol. (2011) 412, 267–284

Contents lists available at www.sciencedirect.com

Journal of Molecular Biology

journal homepage: http://ees.elsevier.com.jmb

Kinetic Recognition of the Retinoblastoma Tumor Suppressor by a Specific Protein Target

Lucía B. Chemes[1], Ignacio E. Sánchez[2] and Gonzalo de Prat-Gay[1]*

[1]*Protein Structure–Function and Engineering Laboratory, Fundación Instituto Leloir and IIBBA-CONICET, Avenida Patricias Argentinas 435, 1405 Buenos Aires, Argentina*
[2]*Protein Physiology Laboratory, Departamento de Quimica Biologica, Facultad de Ciencias Exactas y Naturales, Universidad de Buenos Aires, C1428EGA Buenos Aires, Argentina*

Received 23 May 2011;
received in revised form
4 July 2011;
accepted 11 July 2011
Available online
21 July 2011

Edited by J. E. Ladbury

Keywords:
retinoblastoma protein;
viral oncoprotein;
LxCxE motif;
phosphorylation;
intrinsically disordered proteins

The retinoblastoma tumor suppressor (Rb) plays a key role in cell cycle control and is linked to various types of human cancer. Rb binds to the LxCxE motif, present in a number of cellular and viral proteins such as AdE1A, SV40 large T-antigen and human papillomavirus (HPV) E7, all instrumental in revealing fundamental mechanisms of tumor suppression, cell cycle control and gene expression. A detailed kinetic study of RbAB binding to the HPV E7 oncoprotein shows that an LxCxE-containing E7 fragment binds through a fast two-state reaction strongly favored by electrostatic interactions. Conversely, full-length E7 binds through a multistep process involving a pre-equilibrium between E7 conformers, a fast electrostatically driven association step guided by the LxCxE motif and a slow conformational rearrangement. This kinetic complexity arises from the conformational plasticity and intrinsically disordered nature of E7 and from multiple interaction surfaces present in both proteins. Affinity differences between E7N domains from high- and low-risk types are explained by their dissociation rates. In fact, since Rb is at the center of a large protein interaction network, fast and tight recognition provides an advantage for disruption by the viral proteins, where the balance of physiological and pathological interactions is dictated by kinetic ligand competition. The localization of the LxCxE motif within an intrinsically disordered domain provides the fast, diffusion-controlled interaction that allows viral proteins to outcompete physiological targets. We describe the interaction mechanism of Rb with a protein ligand, at the same time an LxCxE-containing model target, and a paradigmatic intrinsically disordered viral oncoprotein.

Introduction

The retinoblastoma tumor suppressor (Rb) protein plays a central role in the control of cell cycle progression, development, differentiation and chromatin structure.[1–3] Rb is functionally inactivated in a wide range of human tumors[4] and is targeted by several oncogenic viruses, leading to cell transformation.[5] Rb is an adaptor protein reported to associate to over 100 targets[6] that functions as hub

*Corresponding author. E-mail address: gpg@leloir.org.ar.

Abbreviations used: HPV, human papillomavirus; CKII, casein kinase II; FITC, fluorescein isothiocyanate; TSE, transition-state ensemble; HDAC, histone deacetylase.

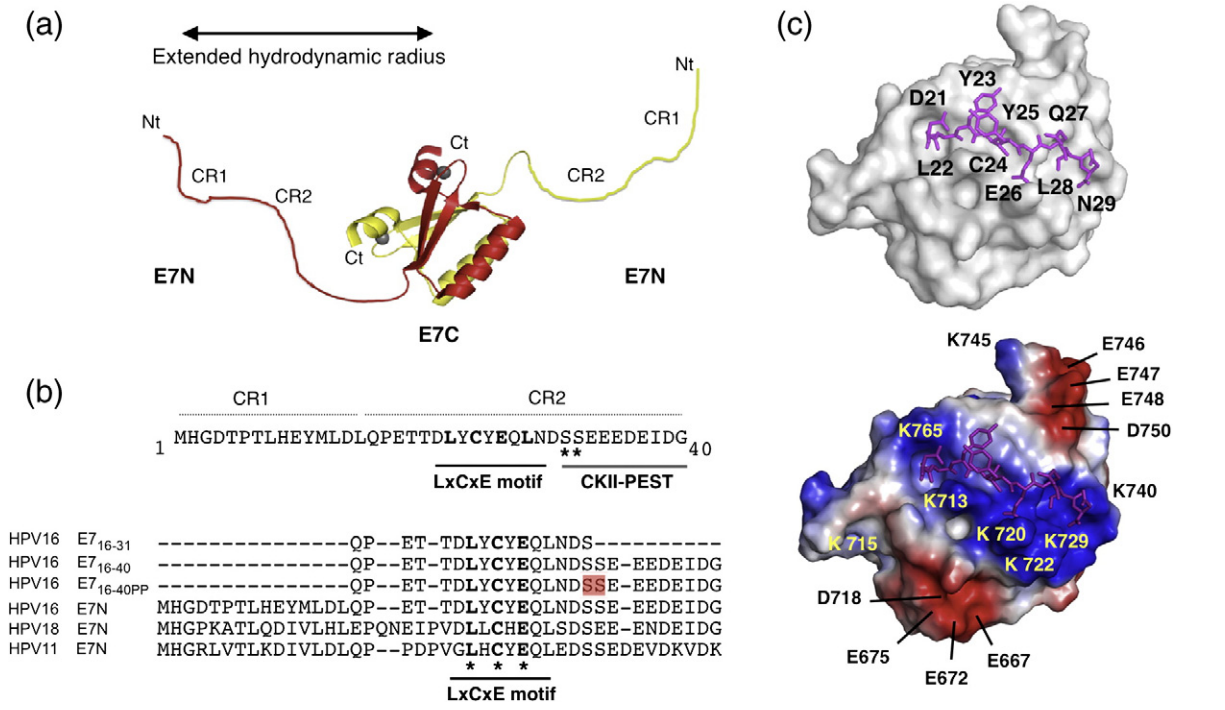

Fig. 1. Structural features of the HPV E7 protein and the E7 LxCxE:Rb interaction. (a) Scheme of the HPV E7 dimer and its E7N and E7C domains (The E7C domain structure is from Protein Data Bank ID: 2B9D). Monomers are depicted in red and yellow, respectively. CR1 and CR2, conserved regions 1 and 2, respectively; Nt, N-terminus; Ct, C-terminus; gray ball, zinc atom. (b) Sequence of the HPV16 E7N domain and E7 fragments used for kinetic studies. Black line: LxCxE motif; gray line: CKII–PEST region. Red box: phosphoserine residues. (c) Structure of the HPV16 $E7_{21–29}$ peptide bound to the RbAB domain (Protein Data Bank ID: 1GUX). Left: surface representation of the RbB subdomain and stick representation of the LxCxE peptide; peptide residues are shown in boldface. Right: electrostatic potential surface representation showing the location of conserved positively charged (yellow letters) and negatively charged (black letters) surface residues.

of a large protein–protein interaction network.[7] Control of the G1/S transition is mediated through binding of Rb to E2F, which leads to inhibition of the transcriptional activity of different members of the E2F/DP family.[3] Rb also interacts with and regulates the function of proteins from the chromatin remodeling machinery including histone deacetylases (HDACs) $HDAC_{1,2}$, histone methylase Suv39h1 and the regulatory subunit of the condensin II complex hCAP-D3.[2,8]

The RbAB domain (residues 380–787) contains two highly conserved protein-binding surfaces: the E2F site, which is targeted by the E2F transactivation ($E2F^{TD}$) domain,[9,10] and the LxCxE cleft, which is the binding site for the HDAC protein[11] and several other cellular LxCxE-containing Rb targets.[12] Ligand exchange at both sites is important for Rb function. Upon phosphorylation, intramolecular interactions of the RbAB flexible linker with the E2F site[13] and of the RbC domain with the LxCxE cleft[14] lead to E2F displacement. The LxCxE linear motif is an interaction module widely disseminated among many eukaryotic DNA[15] and RNA[16–18] viruses that serves virus replication, allowing targeting of cell cycle control regulated by the retinoblastoma protein.[19] Human papillomavirus (HPV) E7,[20] SV40 large T antigen[21] and adenovirus E1A[22] use the LxCxE motif as a high-affinity anchor for Rb binding. Docking to the LxCxE cleft allows interactions with additional Rb surfaces, such as that of the adenovirus E1A CR1 region with the E2F site,[23] which lead to E2F displacement.[24,25]

The thermodynamics and kinetics of protein–protein interactions determine ligand exchange dynamics and therefore strongly influence protein network function. For example, modest changes in the stability[26] or dynamics[27] for formation of key complexes in the Ras–effector network can have a strong effect on cell phenotype. Knowledge of the dynamics and mechanisms of ligand exchange at the LxCxE cleft is essential for understanding the competition established between viral and cellular proteins that target this surface and, in particular, the interfering effect that E7 will have on the Rb regulatory network upon viral infection or oncogenic over-expression. This implies quantifying the binding stability, measuring the timescales for association and dissociation and identifying intermediate species and the kinetic routes connecting them.[28] Nevertheless, structural information is available for only a few

LxCxE-containing proteins,[11,20,21] and knowledge of their kinetics and mechanism of interaction is still lacking.

HPV E7 is a prototypical viral oncoprotein linked to cancer by its strong transforming properties,[29] which also impairs pocket protein function upon natural expression.[30] These effects depend critically on the ability of E7 to promote the dissociation of endogenous complexes between pocket proteins and their cellular partners. HPV16 E7 consists of an intrinsically disordered N-terminal domain (E7N, residues 1–40) that contains the LxCxE motif[31–33] and of a folded C-terminal domain (E7C, residues 41–98) responsible for Zn^{2+} binding and protein dimerization[34,35] (Fig. 1a). The primary interaction between E7 and Rb occurs through a nanomolar affinity interaction between the LxCxE motif (residues 21–29) of E7 and the LxCxE cleft in the RbAB domain (Fig. 1b and c).[20,36] Residues 21–29 are disordered in free E7[31] yet adopt a well-defined extended conformation in the complex,[20] making this a coupled folding and binding event. The acidic casein kinase II (CKII)–PEST region (residues 30–40, Fig. 1b) harbors two CKII phosphorylation sites (S31 and S32), which increase Rb binding affinity,[36] and a PEST degradation signal.[37] Site-directed mutagenesis of the E7 CKII–PEST region and of a patch of highly conserved lysines on the surface of RbAB (Fig. 1c) impairs E7:RbAB binding, suggesting that these complementary charged residues established ionic interactions.[38] The conserved lysines in RbAB are also required for the association with cellular LxCxE-containing proteins.[39] The presence of a negatively charged residue immediately preceding the motif determines the differences in affinity between high-risk and low-risk E7 proteins[40] and between the LxCxE motifs of E7 and the cellular HDAC protein,[11] but the role of electrostatic contacts in the E7:Rb interaction has not been assessed. The additional regions of E7 that participate in Rb binding include an interaction between the E7C domain and the RbC domain, which is required for E2F displacement,[25,34,41] and interactions of the E7C domain and the E7 CR1 region with RbAB, which target additional interaction surfaces of this domain.[36] The E7C domain increases E7 monomer affinity for RbAB by 10-fold, while the E7 CR1 region does not contribute to Rb binding by the E7 monomer.[36] Differences in the transforming properties of prototypical high- and low-risk E7 proteins (HPV16 and HPV18 *versus* HPV11 and HPV6)[42] are related to changes in Rb interaction affinity, with high-risk E7 proteins binding with higher affinity than their low-risk counterparts.[36,40]

E7 is an extended, structurally flexible dimer in solution (Fig. 1a) that can adopt a compact conformation in low concentrations of GdmCl[33] and can undergo structural transitions upon mild changes in the chemical environment.[31,33] Intrinsic disorder and conformational plasticity within E7 are thought to expand its interaction repertoire[31,33,43,44] and may allow for flexibility and speed[45] in accommodating the several interaction surfaces that participate in binding to Rb, but the influence of multiple binding sites and structural flexibility on the mechanism of interaction with Rb has not been explored to date. Other LxCxE-containing Rb partners also present multiple interaction sites, including viral proteins AdE1A and SV40-LT and cellular targets HDAC, EID-1 and CtIP,[11,46–51] stressing the need for understanding their role on the interaction mechanism.

Recombinant expression and purification of Rb domains have proven to be a challenging task, and to date, there are no structural or biophysical studies of full-length Rb. Large multidomain proteins such as Rb can be tackled by the domain approach, where studies of individual domains set the basis for studies involving larger protein fragments, as shown with great success for the P53 tumor suppressor.[52] We have chosen the RbAB domain, which contains the primary E7 interaction site, as a starting point for studying the Rb:E7 interaction mechanism. In the present work, we combined stopped-flow fluorimetry, equilibrium measurements, peptide mapping and quantitative modeling to perform a detailed kinetic study of the interaction between HPV E7 and the RbAB domain in solution. Our results provide insights for understanding the mechanisms through which viral proteins such as HPV E7 efficiently interfere with the Rb interaction network and reveal features of a coupled folding and binding reaction involving an intrinsically disordered viral protein.

Results

Measurement of E7:RbAB association kinetics

In order to study the mechanism of association between the HPV E7 protein and the RbAB domain, we used a series of N-terminally fluorescein isothiocyanate (FITC)-labeled synthetic peptides corresponding to different E7 regions (Fig. 1b) or FITC-labeled recombinant full-length E7 protein. Measurements were performed in reaction buffer containing 20 mM sodium phosphate (pH 7.0), 200 mM NaCl, 1 mM DTT and 0.1% Tween 20 at 20 ± 0.1 °C, where the binding reaction is fully reversible and yields a stable complex.[36] Association and dissociation reactions were monitored through changes in fluorescence intensity or anisotropy of the FITC moiety coupled to the E7 fragments, and time traces were acquired by using a stopped-flow fluorimeter or a fluorescence spectrometer

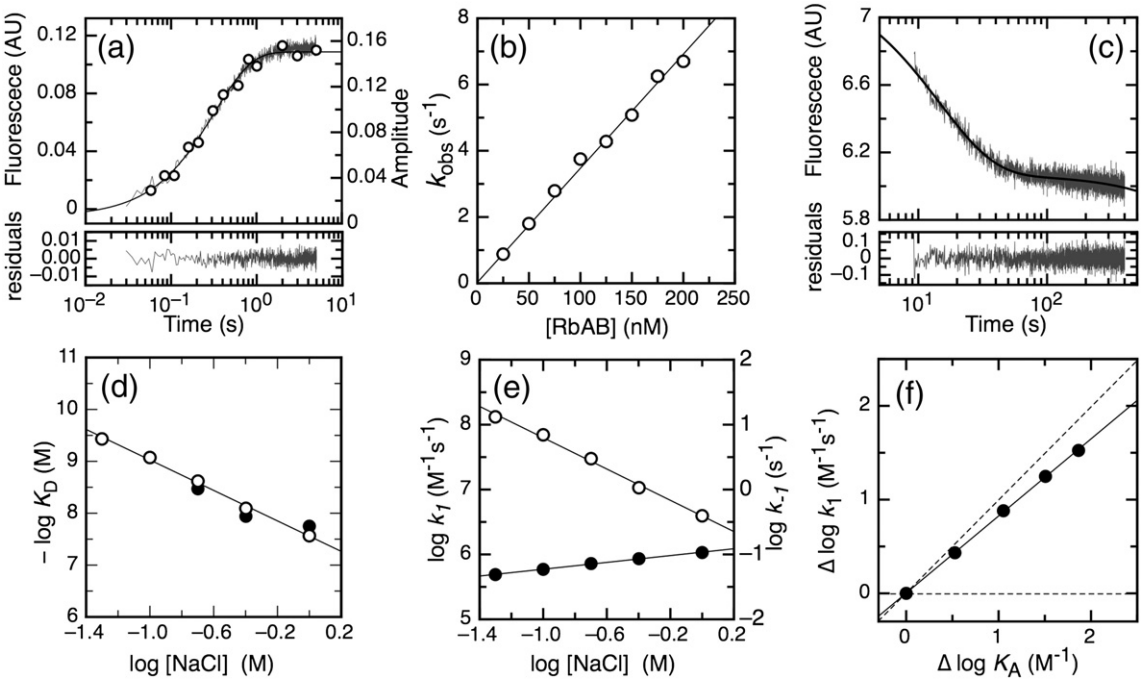

Fig. 2. Kinetics and NaCl dependence of the interaction between the E7 LxCxE motif and the RbAB domain. (a) Association trace recorded after mixing 5 nM FITC-$E7_{16–31}$ with 50 nM RbAB and fit to a mono-exponential function, with $k_{obs} = 3.01 \pm 0.04\ s^{-1}$. (○) Amplitude of the dissociation phase at different delay times measured in an interrupted association experiment; a mono-exponential fit gave $k = 3.10 \pm 0.28\ s^{-1}$. (b) Observed association rate constant (k_{obs}) as a function of RbAB concentration at fixed 5-nM FITC-$E7_{16–31}$ concentration. Data were fit to a linear function ($R^2 = 0.997$; slope $= 3.44 \pm 0.02 \times 10^{-2}\ nM^{-1}\ s^{-1}$; intercept $= 0.023 \pm 0.009\ s^{-1}$). (c) Dissociation trace recorded after adding 1.25 μM unlabeled $E7_{16–31}$ peptide to a stoichiometric complex of 25 nM [FITC-$E7_{16–31}$:RbAB]. Data were fit to a mono-exponential function with slope obtaining, for this trace, a value of $k_{off} = 0.067 \pm 0.001\ s^{-1}$. (d) NaCl dependence of the equilibrium dissociation constant obtained from kinetic (○) or equilibrium (●) measurements. (e) NaCl dependence of the kinetic association (○) and dissociation (●) rate constant. (f) Rate–equilibrium free-energy plot for the effect of NaCl on the $E7_{16–31}$:RbAB interaction. Data from plots (d) to (f) were fit to linear functions with $R^2 > 0.99$, and the Γ_{NaCl} values are reported in Table 2.

depending on the timescales of the binding reactions. The dissociation constant of the E7 dimer has been estimated to be 1 μM by analytical ultracentrifugation.[53] Therefore, under the measurement conditions (low nanomolar concentrations), it is safe to assume that the E7 protein was monomeric. The RbAB domain and E7 peptide fragments were also monomeric in the concentration range assayed (see Materials and Methods).

The HPV16 E7 LxCxE motif binds to RbAB through a two-state association route

We have previously mapped the energetic contribution of different regions of the HPV16 E7 protein to RbAB binding, showing that the LxCxE motif constitutes the main binding determinant and accounts for 90% of the total free-energy of interaction.[36] In order to study RbAB association

Table 1. Kinetic rate constants for the interaction between RbAB and E7N fragments

Fragment	k_{on} ($M^{-1}\ s^{-1}$)	k_{off} (s^{-1})	$K_{d(kin)}$[a] (M)	$K_{d(eq)}$[b,c] (M)
HPV16 $E7_{16–31}$	$3.44 \pm 0.02 \times 10^7$	0.072 ± 0.001	$2.10 \pm 0.03 \times 10^{-9}$	$5.1 \pm 1.3 \times 10^{-9}$[b]
HPV16 $E7_{16–40}$	$2.33 \pm 0.01 \times 10^7$	0.073 ± 0.001	$3.13 \pm 0.05 \times 10^{-9}$	$6.5 \pm 1.0 \times 10^{-9}$[b]
HPV16 $E7_{16–40PP}$	$1.40 \pm 0.30 \times 10^8$	0.050 ± 0.004	$0.36 \pm 0.08 \times 10^{-9}$	$1.8 \pm 0.4 \times 10^{-9}$[b]
HPV16 $E7_{1–40}$	$2.50 \pm 0.10 \times 10^7$	0.066 ± 0.001	$2.60 \pm 0.10 \times 10^{-9}$	$3.0 \pm 1.6 \times 10^{-9}$[c]
HPV11 $E7_{1–42}$	$3.10 \pm 0.30 \times 10^7$	3.30 ± 0.10	$110 \pm 10 \times 10^{-9}$	$102 \pm 25 \times 10^{-9}$[c]
HPV18 $E7_{1–43}$	$2.41 \pm 0.06 \times 10^7$	0.270 ± 0.002	$11.2 \pm 0.3 \times 10^{-9}$	$3.3 \pm 0.3 \times 10^{-9}$[c]

All measurements were performed at 200 mM [NaCl] and 20 ± 1 °C.
[a] $K_{d(kin)}$ was calculated as k_{off}/k_{on}.
[b] $K_{d(eq)}$ data are from Ref. 36.
[c] $K_{d(eq)}$ data were determined as explained in Materials and Methods and Supplementary Fig. 4.

$$E7_{16\text{-}31} + RbAB \underset{k_{off} = 0.072 \pm 0.001\ s^{-1}}{\overset{k_{on} = 3.44 \pm 0.02\ 10^7\ M^{-1}s^{-1}}{\rightleftharpoons}} [E7_{16\text{-}31}{:}RbAB]$$

Scheme 1. Kinetic association route for the [$E7_{16\text{-}31}$:RbAB] complex.

kinetics, we used the FITC-labeled $E7_{16–31}$ fragment, which contains the LxCxE motif (Fig. 1b). We measured the increase in FITC fluorescence produced after mixing solutions containing a fixed amount of FITC-labeled $E7_{16\text{-}31}$ and varying concentrations of RbAB. All association traces in pseudo-first-order regime showed a mono-exponential increase in fluorescence with time (Fig. 2a), indicating the presence of a single association event. Furthermore, the observed association rate (k_{obs}) increased linearly with increasing RbAB concentration, confirming the bimolecular nature of the association reaction (Fig. 2b).

In order to measure the dissociation rate, we first assembled a stoichiometric 25-nM [$E7_{16–31}$:RbAB] complex using FITC-labeled peptide. After equilibration, dissociation was produced by adding an excess amount of unlabeled $E7_{16–31}$ peptide. Addition of the unlabeled ligand produced a decrease in the fluorescence signal to a value undistinguishable from that of the unbound probe, verifying that the association reaction was fully reversible (data not shown). Dissociation traces showed a mono-exponential decay, indicating the presence of a single dissociation event (Fig. 2c).

The presence of a single association phase in pseudo-first-order regime, the linear dependence of k_{obs} on RbAB concentration and the presence of a single dissociation phase are compatible with a two-state reaction. The microscopic association rate constant calculated from the pseudo-first-order plot was $k_{on} = 3.44 \pm 0.02 \times 10^7\ M^{-1}\ s^{-1}$ (see Materials and Methods and Table 1). The dissociation rate constant was calculated by averaging the rates obtained by fitting several dissociation traces to a mono-exponential decay (Fig. 2c), obtaining $k_{off} = 0.072 \pm 0.001\ s^{-1}$ (Table 1), and by extrapolating the intercept of the pseudo-first-order plot (Fig. 2b), obtaining $k_{off} = 0.023 \pm 0.009\ s^{-1}$. Because of the small value of k_{off}, the estimation obtained from the dissociation trace was considered more exact than that obtained by extrapolation. The equilibrium dissociation constant calculated from the kinetic rate constants considering a two-state reaction was $K_d = k_{off}/k_{on} = 2.1 \pm 0.03 \times 10^{-9}$ M, in excellent agreement with the value of $5.1 \pm 1.3 \times 10^{-9}$ M obtained from equilibrium titration experiments[36] (Table 1). We followed the formation of the final complex in an interrupted "double-jump" association experiment (see Materials and Methods). In this experiment, we mixed 10 nM FITC- labeled $E7_{16–31}$ with 50 nM RbAB. After varying delay times, we added an excess 2. 5-μM amount of unlabeled $E7_{16–31}$ peptide and measured the resulting dissociation kinetics. At all delay times, we found a single dissociation phase with an average rate constant of $k_{off} = 0.054 \pm 0.002\ s^{-1}$, corresponding to the dissociation of the [$E7_{16–31}$:RbAB] complex (Table 1). The amplitude of this phase is proportional to the concentration of the [$E7_{16–31}$:RbAB] complex. This complex was formed with an apparent rate constant $k_{obs} = 3.10 \pm 0.28\ s^{-1}$ (Fig. 2a, open circles), which was in excellent agreement with the rate measured in the direct association experiment, $k_{obs} = 3.01 \pm 0.04\ s^{-1}$ (Fig. 2a, line trace). This agreement provided additional evidence that the HPV16 $E7_{16–31}$ fragment associates with the RbAB domain following a two-state route with no detectable intermediates, according to Scheme 1.

Ionic strength dependence of the HPV16 $E7_{16–31}$:RbAB interaction

A thermodynamic signature of electrostatic interactions is their sensitivity to variation of the ionic strength, since high salt concentrations screen charge–charge interactions.[54] We performed equilibrium titrations and kinetic measurements in reaction buffer containing varying NaCl concentrations in order to analyze the contribution of electrostatic interactions to the formation of the [$E7_{16–31}$:RbAB] complex. Equilibrium titrations were performed at NaCl concentrations equal or higher than 0.2 M (Supplementary Fig. 1a), since at lower [NaCl], we observed slow precipitation of the complex. The association rate constant at each [NaCl] was calculated as $k_{on} = (k_{obs} - k_{off})/[RbAB]$, and the k_{off} values were determined from dissociation traces obtained by addition

Table 2. NaCl dependence of the equilibrium and rate constants for RbAB:E7N interactions

Fragment	Γ^{EQ}_{NaCl}	Γ^{on}_{NaCl}	Γ^{off}_{NaCl}	α_{NaCl}
HPV16 $E7_{16–31}$	−1.47 ± 0.05	−1.20 ± 0.05	0.26 ± 0.01	0.82 ± 0.01
HPV16 $E7_{16–40}$	−1.82 ± 0.07	−1.56 ± 0.03	0.26 ± 0.04	0.85 ± 0.02
HPV16 $E7_{16–40PP}$	−2.43 ± 0.07	−1.86 ± 0.08	0.57 ± 0.06	0.76 ± 0.02
HPV16 $E7_{1–40}$	−1.60 ± 0.12	−1.31 ± 0.14	0.30 ± 0.04	0.82 ± 0.03
HPV11 $E7_{1–42}$	−1.44 ± 0.07	−1.40 ± 0.06	0.03 ± 0.04[a]	0.98 ± 0.03
HPV18 $E7_{1–43}$	−1.42 ± 0.11	−1.27 ± 0.11	0.14 ± 0.01	0.90 ± 0.01

All reported values were obtained from linear fits with R2 > 0.99 except noted otherwise.
[a] R2 = 0.17

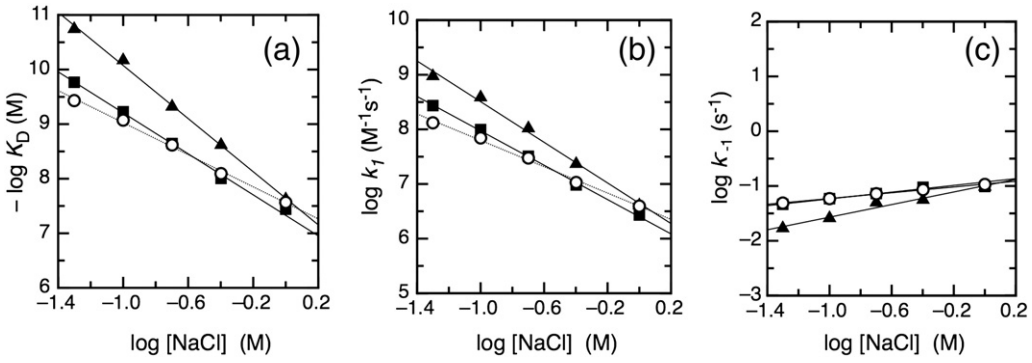

Fig. 3. NaCl dependence of the equilibrium and kinetic rate constants for the interaction between RbAB and $E7_{16–40}$ or $E7_{16–40PP}$. NaCl dependence of the equilibrium dissociation constant (a) and the kinetic association (b) and dissociation (c) rate constants for the interaction between RbAB and the $E7_{16–40}$ (■) and $E7_{16–40PP}$ (▲) peptides. Data for $E7_{16–31}$ (○) are shown for comparison. The data were fit to linear functions with $R^2 > 0.99$, and the Γ_{NaCl} parameters obtained from the fits are reported in Table 2.

of excess unlabeled ligand. Kinetic traces were mono-exponential at all NaCl concentrations (Supplementary Fig. 1b and c), and there was a good agreement between the K_d value obtained from kinetic (Fig. 2d, open circles) and equilibrium (Fig. 2d, filled circles) measurements, indicating that the reaction did not deviate from a two-state route.

The magnitude of variation in the equilibrium and rate constants produced by variations in [NaCl] can be characterized by the slope of $-\log K_d$ (or $\log K_a$), $\log k_{on}$ and $\log k_{off}$ *versus* $\log$ [NaCl], also referred to as $\Gamma^{EQ}{}_{NaCl}$, $\Gamma^{on}{}_{NaCl}$ and $\Gamma^{off}{}_{NaCl}$:[55,56]

$$\Gamma^{EQ}_{NaCl} = -\frac{\partial \log K_d}{\partial \log[NaCl]} = \frac{\partial \log K_a}{\partial \log[NaCl]}$$

$$\Gamma^{on}_{NaCl} = \frac{\partial \log k_{on}}{\partial \log[NaCl]}; \Gamma^{off}_{NaCl} = \frac{\partial \log k_{off}}{\partial \log[NaCl]}$$

A negative value of $\Gamma^{EQ}{}_{NaCl}$ and $\Gamma^{on}{}_{NaCl}$ and a positive value of $\Gamma^{off}{}_{NaCl}$ indicate that the complex is destabilized upon an increase in [NaCl].

An increase of 1 order of magnitude in [NaCl] produced a 70-fold increase in the K_d value, corresponding to a 2.5 ± 0.1 kcal mol^{-1} decrease in the stability of the [$E7_{16–31}$:RbAB] complex (Fig. 2d and $\Gamma^{EQ}{}_{NaCl} = -1.47 \pm 0.05$, Table 2). This effect was due mainly to a decrease in k_{on} (Fig. 2e, open circles; $\Gamma^{on}{}_{NaCl} = -1.20 \pm 0.05$, Table 2), with a minor contribution due to a modest increase in k_{off} (Fig. 2e, filled circles; $\Gamma^{off}{}_{NaCl} = 0.26 \pm 0.01$, Table 2).

The α_{NaCl} parameter is defined as the ratio of the rate of variation of $\log$ (k_{on}) upon a variation in $\log$ [NaCl] with respect to the rate of variation of $\log$ (K_a) upon a variation in $\log$ [NaCl]:

$$\alpha_{NaCl} = \frac{\partial \log(k_{on}) / \partial \log[NaCl]}{\partial \log(K_a) / \partial \log[NaCl]} = \frac{\Gamma^{on}_{NaCl}}{\Gamma^{EQ}_{NaCl}}$$

This parameter measures the proportion of the variation in the total free energy of interaction produced by salt that is reflected as a variation in the free energy of activation for the association process. In the simplest case, α_{NaCl} takes values between 0 and 1, with a value of 1 indicating that the probed interactions are fully established in the transition-state ensemble (TSE) and a value of 0 indicating that the interactions are not present in the TSE.

The [$E7_{16–31}$:RbAB] complex had a value of $\alpha_{NaCl} = 0.82 \pm 0.01$ (Fig. 2f and Table 2), indicating that the complex is stabilized by electrostatic interactions that are, to a large extent, established in the TSE and contribute to complex formation by speeding up association.

Contribution of the CKII–PEST region to RbAB binding

The CKII–PEST region of E7, which lies proximal to the LxCxE motif, is conserved and contains a high proportion of negatively charged residues (Fig. 1b) previously proposed to contribute to RbAB binding.[38] In order to test for this possibility, we measured the [NaCl] dependence of the equilibrium and rate constants for the interaction between RbAB and the $E7_{16–40}$ peptide, which contains both the LxCxE motif and the CKII–PEST region (Fig. 1b). Binding kinetics were mono-exponential, with a linear dependence of k_{obs} on RbAB concentration (Supplementary Fig. 2a–c). The K_d values determined from kinetic measurements and from equilibrium titrations were in excellent agreement (Table 1), confirming that association followed a two-state reaction.

At 0.05 M NaCl, the presence of the CKII–PEST region increased the binding free energy by 0.45 kcal mol^{-1}. The presence of the CKII–PEST region also increased $\Gamma^{EQ}{}_{NaCl}$ from -1.47 ± 0.05 for $E7_{16–31}$ to -1.82 ± 0.07 for $E7_{16–40}$ (Fig. 3a and Table 2). These results indicated that the CKII–PEST region contributed with stabilizing interactions, which were of electrostatic nature.

The increase in Γ^{EQ}_{NaCl} was due to a stronger dependence of k_{on} on [NaCl] for the $E7_{16–40}$ peptide, while the Γ^{off}_{NaCl} value did not change (Fig. 3b and c and Table 2). In analogy to the Φ value used to analyze the effect of point mutations,[57] it is possible to define a $\phi_{CKII–PEST}$ value, which measures the extent to which the interactions contributed by the CKII–PEST region are established in the TSE:

$$\phi_{CKII-PEST} = \frac{\Delta G^{ON,\ddagger}_{16-40} - \Delta G^{ON,\ddagger}_{16-31}}{\Delta G^{EQ}_{16-40} - \Delta G^{EQ}_{16-31}}$$

A $\phi_{CKII–PEST}$ value of 1 implies that the interactions contributed by the CKII–PEST region are fully established in the TSE, while a value of 0 indicates that the interactions are formed after the TSE. Similar $\phi_{CKII–PEST}$ values were obtained at different [NaCl] concentrations (data not shown). At 0.05 M NaCl, where the energetic contribution of this region was strongest, the $\Phi_{CKII–PEST}$ value was 0.92 ± 0.03 (Table 2). Therefore, we can conclude that the stabilizing electrostatic interactions contributed by the CKII–PEST region are established in the TSE.

Effect of E7 phosphorylation at S31 and S32 on RbAB binding kinetics

Phosphorylation of the serine residues located within the CKII–PEST region of E7 is required for the induction of S-phase reentry in HPV-infected differentiating keratinocytes[58] as well as for E7 transforming properties,[59] two effects known to be mediated through interaction of E7 with pocket proteins. Recently, E7 phosphorylation was shown to increase p130[60] and RbAB binding affinity.[36] In order to analyze the effect of phosphorylation on the interaction kinetics, we measured the binding kinetics between RbAB and the HPV16 $E7_{16–40PP}$ peptide, which is phosphorylated at S31 and S32 (Fig. 1b). Complex formation occurred through a two-state route, as shown by the mono-exponential kinetics of the binding reaction, the linear dependence of k_{obs} on RbAB concentration (Supplementary Fig. 2d–f) and the agreement between the K_d values determined from kinetic and equilibrium measurements (Table 1).

At 0.05 M NaCl, phosphorylation had a stabilizing effect on complex formation, increasing the binding

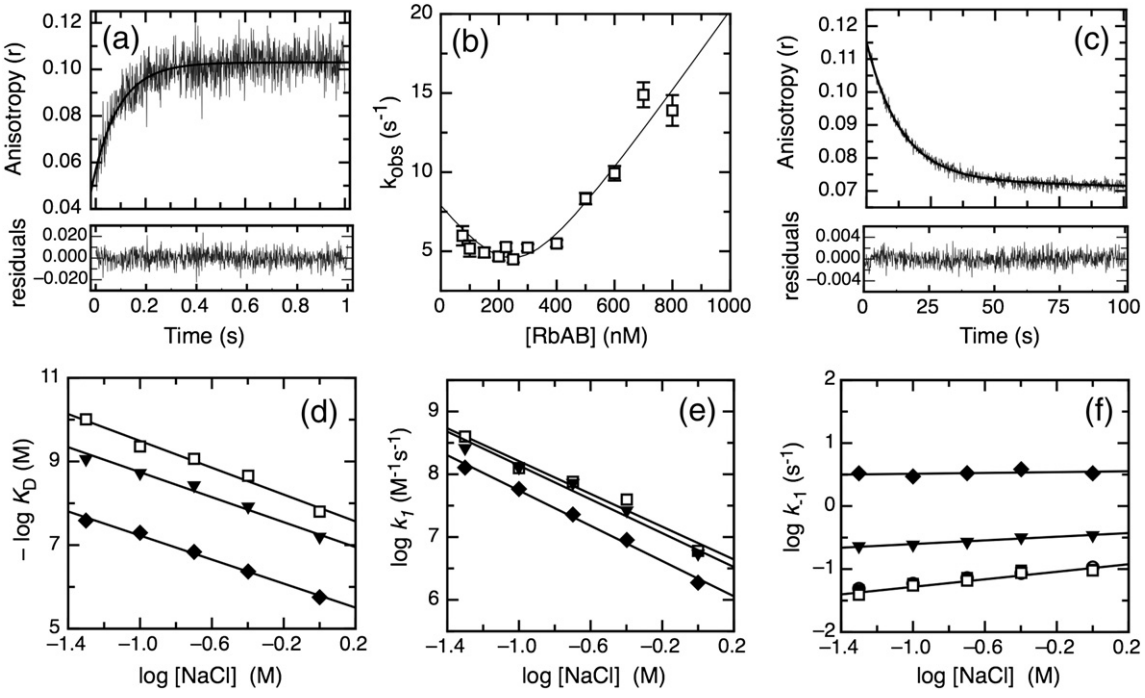

Fig. 4. Binding kinetics and NaCl dependence of the E7N:RbAB interaction from prototypical high- and low-risk E7 proteins. (a) Kinetic association trace measured by mixing 200 nM FITC-labeled HPV16 E7N with 800 nM RbAB. The trace was fit to a single-exponential function, with $k_{obs} = 9.48 \pm 0.41\ s^{-1}$. (b) Dependence of the observed association rate constant (k_{obs}) on RbAB concentration at a fixed concentration of 200 nM FITC-labeled HPV16 E7N. The data were fit to a previously described model [see Eq. (3)] to obtain the value of $k_{on} = 2.5 \pm 0.1 \times 10^7\ M^{-1}\ s^{-1}$. (c) Kinetic dissociation trace measured after adding 8 μM unlabeled HPV16 E7N peptide to a preformed complex of 200 nM FITC-labeled E7N and 400 nM RbAB. The trace was fit to a single-exponential function, obtaining $k_{off} = 7.00 \pm 0.06 \times 10^{-2}\ s^{-1}$. Kinetic parameters for the E7N:RbAB interaction are reported in Table 1. (d–f) NaCl dependence of the equilibrium constant (d) and of the kinetic association (e) and dissociation (f) rate constants for different E7N domains. The Γ_{NaCl} parameters obtained from the linear fits of the data are reported in Table 2 ($R^2 > 0.99$ except as noted). E7N domains: HPV16 E7N (□), HPV18 E7N (▼), HPV11 E7N (♦). In panel (f) the data for HPV16 $E7_{16-40}$ is shown for comparison (■).

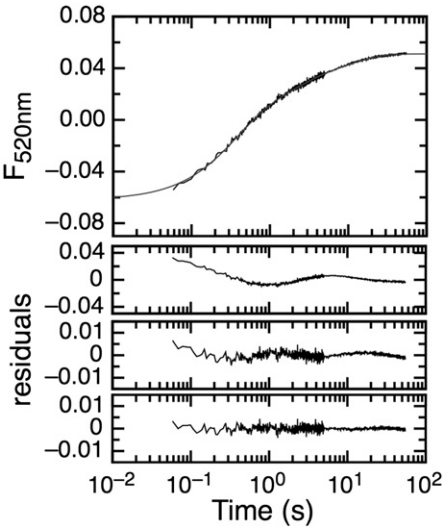

Fig. 5. Association kinetics between full-length E7 and RbAB. Fluorescence intensity change produced after mixing 5 nM FITC-E7 and 100 nM RbAB in measurement buffer containing 200 mM [NaCl]. The residuals from fits to single-exponential (upper), double-exponential (middle) and triple-exponential (lower) functions are shown below the graph. For this trace, the fitted rate constants were $k_{obs1} = 5.2 \pm 0.2\ s^{-1}$, $k_{obs2} = 1.12 \pm 0.04\ s^{-1}$ and $k_{obs3} = 0.124 \pm 0.003\ s^{-1}$.

free energy by 1.31 ± 0.05 kcal mol^{-1} with respect to the unphosphorylated $E7_{16-40}$ fragment. Phosphorylation also increased the $\Gamma^{EQ}{}_{NaCl}$ value from -1.82 ± 0.07 to -2.43 ± 0.07 (Fig. 3a and Table 2), due to changes in both $\Gamma^{on}{}_{NaCl}$ and $\Gamma^{off}{}_{NaCl}$ (Fig. 3b and c and Table 2). The $\Phi_{PHOSPHO}$ value, defined as:

$$\phi_{PHOSPHO} = \frac{\Delta G^{ON,\ddagger}_{16-40PP} - \Delta G^{ON,\ddagger}_{16-40}}{\Delta G^{EQ}_{16-40PP} - \Delta G^{EQ}_{16-40}}$$

was similar at different NaCl concentrations. At 0.05 M [NaCl], where the contribution due to phosphorylation was strongest, $\Phi_{PHOSPHO}$ was 0.56 ± 0.04 (Table 2). These results indicated that phosphorylation contributes with stabilizing interactions of electrostatic nature, which are partially established in the TSE.

Differences in binding kinetics of the E7N domains from high- and low-risk E7 proteins

Prototypical low-risk HPV11 and HPV6 E7 proteins bind to RbAB with lower affinity than do high-risk HPV16 and HPV18 E7 proteins[36,61] (Table 1), which is related to their lower transforming potential.[42] To investigate the kinetic basis for these differences, we measured the equilibrium

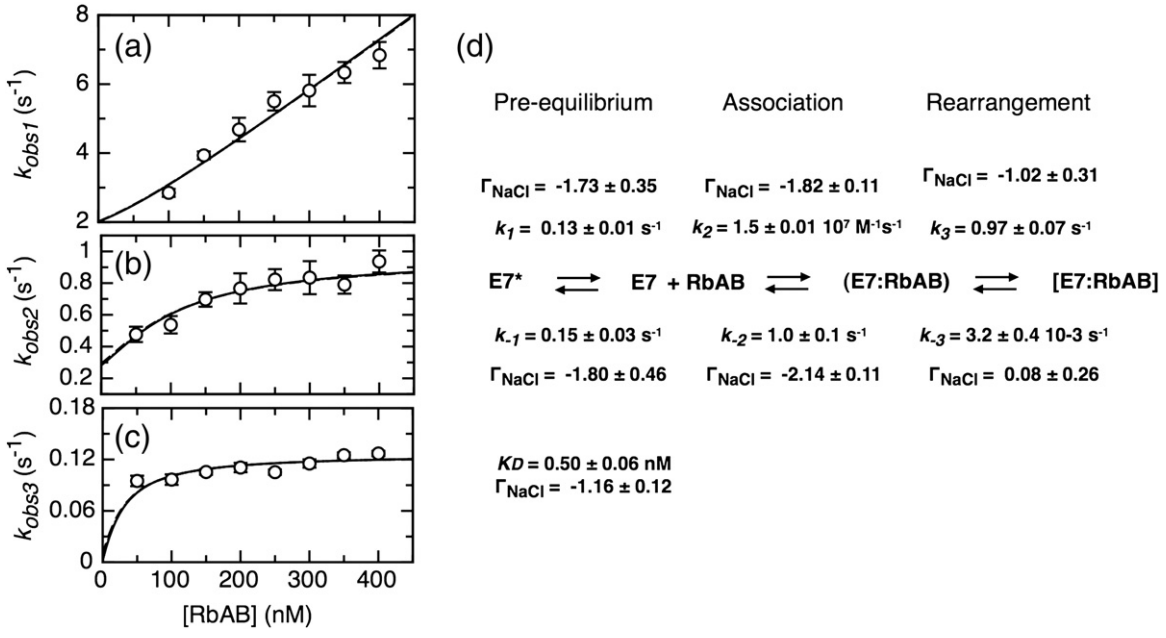

Fig. 6. Quantitative modeling of the E7: RbAB interaction. (a–c) Dependence of the three observed rate constants (k_{obs1}, k_{obs2} and k_{obs3}) on RbAB concentration at 0.2 M NaCl and global fit to the four-state association model shown in Scheme 2 and in (d) and described in the main text and in Supplementary Figs. 5 and 8. (d) Microscopic rate constants at 0.2 M NaCl obtained by the global fit shown in (a) to (c) and corresponding Γ_{NaCl} values. The Γ_{NaCl} values were obtained from the linear fits of the dependence of the microscopic rate constants on NaCl concentration shown in Fig. 7. The K_d value for the E7:RbAB interaction at 0.2 M NaCl and its Γ_{NaCl} value are also shown below the scheme.

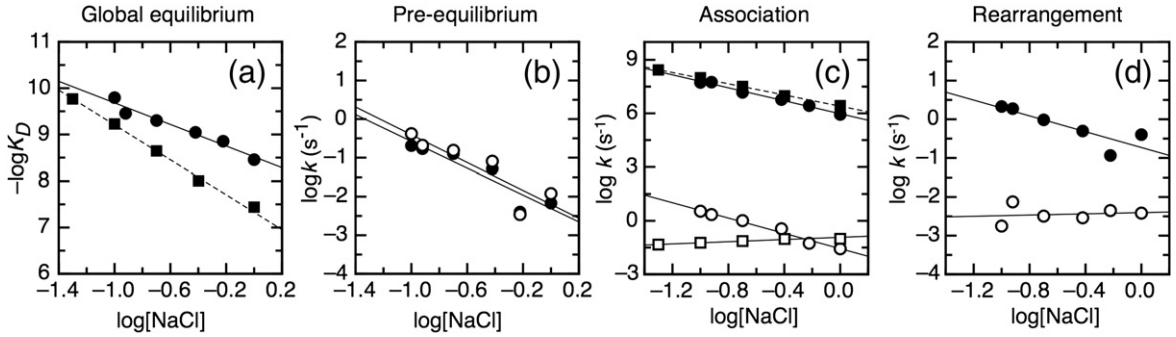

Fig. 7. NaCl dependence of equilibrium and rate constants for the E7:RbAB interaction. (a) NaCl dependence of the equilibrium constant (K_d) for the E7:RbAB and the $E7_{16–40}$:RbAB interactions. (·) E7:RbAB, $\Gamma^{EQ}_{NaCl} = -1.16 \pm 0.12$; (■) $E7_{16–40}$:RbAB, $\Gamma^{EQ}_{NaCl} = -1.82 \pm 0.07$. (b) NaCl dependence of k_1 (●) and k_{-1} (○). (c) NaCl dependence of k_2 (●) and k_{-2} (○). (d) NaCl dependence of k_3 (●) and k_{-3} (○). The values of the microscopic rate constants at each NaCl concentration are reported in Supplementary Table 1 and were obtained from global fits of the observed association rate constants (k_{obs1}, k_{obs2} and k_{obs3}) at each NaCl concentration (see Supplementary Fig. 5). In (c), the NaCl dependences of k_{on} (■) and k_{off} (□) for the $E7_{16–40}$:RbAB interaction are shown for comparison. The data were fit to linear functions, with the corresponding Γ_{NaCl} parameters reported in Fig. 6d.

and rate constants the for interaction between RbAB and the FITC-labeled HPV16, HPV18 and HPV11 E7N domains (Fig. 1b) and their NaCl dependence. We followed the binding reaction by monitoring changes in FITC anisotropy, since none of the E7N domains yielded changes in fluorescence intensity upon RbAB binding. In order to increase the signal-to-noise ratio, we performed measurements at 200 nM FITC-E7N, and association kinetics were measured under non-pseudo-first-order conditions to maintain complex solubility. All association and dissociation traces had mono-exponential kinetics (Fig. 4a and c and Supplementary Fig. 3a, b, d and e). The k_{off} values were obtained as previously described (Table 1), and the k_{on} values were determined [see Eq. (3)] from the k_{obs} *versus* [RbAB] plots (Fig. 4b and Supplementary Fig. 3c and f and Table 1). The agreement between the K_d values determined from kinetic and equilibrium measurements (Table 1 and Supplementary Fig. 4) indicated that all reactions followed a two-state reaction.

All E7N domains showed a decrease in stability upon increasing [NaCl] (Fig. 4d and Table 2), indicating the presence of stabilizing electrostatic interactions. In all cases, the α_{NaCl} values were close to unity, indicating that the electrostatic interactions were present in the TSE (Fig. 4e and f and Table 2). The differences in stability between E7N domains were maintained across different NaCl concentrations (Fig. 4d and Table 2). We defined:

$$\phi_{HPV11E7N} = \frac{\Delta G^{ON,\ddagger}_{HPV11E7N} - \Delta G^{ON,\ddagger}_{HPV16E7N}}{\Delta G^{EQ}_{HPV11E7N} - \Delta G^{EQ}_{HPV16E7N}}$$

$$\phi_{HPV18E7N} = \frac{\Delta G^{ON,\ddagger}_{HPV18E7N} - \Delta G^{ON,\ddagger}_{HPV16E7N}}{\Delta G^{EQ}_{HPV18E7N} - \Delta G^{EQ}_{HPV16E7N}}$$

which allowed us to compare the binding kinetics of the HPV11 and the HPV18 E7N domains with respect to the HPV16 E7N domain. At 0.05 M NaCl, we obtained $\phi_{HPV11E7N} = 0.20 \pm 0.02$ and $\phi_{HPV18E7N} = 0.19 \pm 0.05$, indicating that the differences in stability for both HPV11 and HPV18 E7N with respect to HPV16 E7N were reflected mainly by changes in k_{off} and, therefore, in the half-life of the complexes (Table 2).

Full-length HPV16 E7 binds to RbAB through a multistate route

The E7 protein presents a secondary lower-affinity RbAB binding site located in the E7C domain[36] that may overlap with the previously described RbC binding site, also located in E7C.[25,34] Therefore, we were interested in assessing the influence of this second binding site on the interaction kinetics. Binding between RbAB and the full-length FITC-labeled HPV16 E7 protein at 0.2 M NaCl generated a large change in fluorescence, which was followed by stopped-flow kinetics (Fig. 5). The association traces measured in pseudo-first-order regime did not follow simple kinetics, and fits to a sum of three exponential functions were needed to account for the time traces at all RbAB concentrations tested (Fig. 5). Upon going from 100 to 400 nM RbAB, the faster phase k_{obs1} became 3-fold faster (Fig. 6a), the intermediate phase k_{obs2} became 2-fold faster (Fig. 6b) and the slowest phase k_{obs3} became 1.3-fold faster (Fig. 6c).

The presence of three kinetic phases in the association traces indicates that at least four states need to be considered in order to describe the binding mechanism. There are three such minimal kinetic models. All of them include a bimolecular association event and two unimolecular steps, which may, in

principle, involve isomerization of free E7, of the E7:RbAB complex or of both. All three minimal kinetic models account well for the available experimental data. Since the main conclusions of this work are mechanism independent, we describe in detail the results for one of the three models (Figs. 6 and 7) and show the results for the other two in Supplementary Material (Supplementary Figs. 6 and 7).

We have chosen to highlight a model that considers a pre-equilibrium between two conformations of the E7 protein (E7 and E7*), an association event leading to an intermediate (E7:RbAB) complex and an isomerization step that yields the final consolidated [E7:RbAB] complex (Scheme 2 and Fig. 6d). This model is supported by the available biochemical data on the E7 protein. The N-terminal domain of E7 is disordered in solution, with a heterogeneity that includes α-helical conformations.[31,33] On the other hand, this domain adopts a well-defined, extended conformation in the complex with RbAB.[20] Thus, it is plausible that only a fraction of free E7 molecules are competent for binding. There are two RbAB binding sites in E7, both of which contribute to the binding affinity.[36] An intermediate (E7:RbAB) complex may involve an interaction at only one of the binding surfaces.

First, we fit the [RbAB] dependence of the three observed kinetic association phases to the four-state model at 0.2 M NaCl and restricted the fit by using the K_d value measured independently by equilibrium titrations (Fig. 6a–c). This allowed us to estimate the microscopic rate constants for each reaction step, with standard deviations at or below 10% (Fig. 6d and Supplementary Table 1). Free E7 exists in two similarly populated conformers, which interconvert with rates of about 0.15 s^{-1}. One of these conformers is able to associate to RbAB with a bimolecular association rate very similar to that of the isolated LxCxE motif (Fig. 6d and Table 1). The intermediate complex (E7:RbAB) has lower stability compared to the [$E7_{16–31}$:RBAB] complex, with a K_d of 70 nM (Fig. 6d) compared to 5 nM (Table 1). This intermediate complex then rearranges into the final consolidated complex with a rate constant of 0.9 s^{-1}. The rate constant for the reverse process is 8×10^{-3} s^{-1} (Fig. 6d), an order of magnitude slower than the dissociation rate of the $E7_{16–31}$ fragment (Table 1). This is in accordance with the higher binding affinity of the full-length E7 protein ($K_d = 0.50 \pm 0.06$ nM, Fig. 6d) as compared to the isolated LxCxE motif ($K_d = 5.1 \pm 1.3$ nM, Table 1).

Next, we investigated the salt dependence of the rate constants for each microscopic step. For this purpose, we performed equilibrium and kinetic association experiments at NaCl concentrations ranging from 0.1 to 1 M (Supplementary Fig. 5a). For all salt concentrations tested, three exponential phases were required to fit the association data (data not shown). All observed rate constants became slower at higher salt concentrations (Supplementary Fig. 5b and c). The four-state model of Fig. 6d was able to describe the [RbAB] dependence of the observed kinetic phases at all NaCl concentrations tested (Supplementary Fig. 5a). Each fit was restricted using the K_d value measured at the corresponding NaCl concentration.

The salt dependence of the equilibrium and the microscopic rate constants is displayed in Fig. 7. Surprisingly, the equilibrium constant for the E7:RbAB interaction showed a shallower salt dependence compared to the $E7_{16–40}$ fragment containing the LxCxE motif (Fig. 7a, $\Gamma^{EQ}_{NaCl} = -1.16 \pm 0.12$ *versus* -1.82 ± 0.07). The pre-equilibrium between the two E7 conformers becomes slower at higher salt concentrations for both the forward and the reverse reactions (Fig. 7b). The resulting equilibrium constant is approximately salt independent. In other words, electrostatic interactions do not shift the equilibrium toward either conformation. Interestingly, we observed a similar phenomenon for formation of the intermediate (E7:RbAB) complex (Fig. 7c). The dependence of the association and dissociation rate constants had the same sign and similar magnitude, resulting in a dissociation constant that was nearly salt independent. The association event between E7 and RbAB had a rate constant and salt dependence very similar to those of the $E7_{16–40}$ fragment containing the LxCxE motif and the CKII-PEST region (Fig. 7c). This result strongly suggests that the TSE for association is mainly stabilized by binding of the LxCxE motif and the adjacent CKII–PEST region. On the other hand, the dissociation of the intermediate (E7:RbAB) complex had a salt dependence very different from that of the [$E7_{16–40}$:RbAB] complex (Fig. 7c). There are two possible causes for this phenomenon, not mutually exclusive. One, in the intermediate (E7:RbAB) complex, the E7C domain may form electrostatic interactions in addition to those formed by the $E7_{16–40}$ fragment. Two, the electrostatic interactions formed by the $E7_{16–40}$ fragment in the intermediate (E7:RbAB) complex may be different from those formed by the $E7_{16–40}$ fragment in the [$E7_{16–40}$:RbAB] complex. Finally, the rearrangement of the intermediate (E7:RbAB) complex into the consolidated [E7:RbAB] complex showed a negative salt dependence for the forward reaction, while the reverse step had a null salt dependence (Fig. 7d). As a consequence, electrostatic interactions favor the formation of the final [E7:RbAB] complex from the intermediate (E7:RbAB) complex. The salt dependence of this elementary step ($\Gamma^{EQ}_{NaCl} = -1.1 \pm 0.4$, Fig. 6d) accounts for most of the salt dependence of the complete process ($\Gamma^{EQ}_{NaCl} = -1.16 \pm 0.12$, Fig. 7a).

Discussion

The interaction between E7 and Rb features several properties also found in cellular Rb targets.

First is the presence of the high-affinity LxCxE motif.[12] Second is the presence of several binding sites, for example, in the interaction between Rb and LxCxE-containing cellular partners such as HDAC,[11,47] CtIP[48,49] and EID-1.[50,62]

Binding of the LxCxE module from HPV E7 to RbAB follows a simple two-state route, with no detectable intermediates (Fig. 2). Association is fast ($k_{on}=3\times10^{7}$ M^{-1} s^{-1}). Binding presents a strong electrostatic component that is present in the TSE, suggesting that long-range electrostatic interactions between the complementary charged binding surfaces (Fig. 1c) assist in correct positioning of the LxCxE motif, as found in other electrostatically driven interactions such as Barnase–Barstar,[63] thrombin–hirudin,[64] Ras–Raf[65] and SH2–ligand.[56] This result agrees with mutagenesis data showing that binding of the LxCxE motif from E7 and HDAC to RbAB is favored by the presence of a negatively charged residue preceding the leucine in the motif.[11] The half-life of the complex formed between RbAB and the E7 LxCxE motif is 10 s, within the range observed in other dynamic regulatory interaction modules such as PDZ–ligand,[66] CheY/CheA,[67] Ras–Raf[65] and SH2–ligand[68] and much shorter than that of stable enzyme–inhibitor complexes such as Barnase–Barstar,[63] thrombin–hirudin[64] and AchE–fasciculin.[69] This indicates that even when the interaction between E7 and Rb is tight, association still probably allows for ligand exchange with other cellular proteins at low or intermediate expression levels.

The conserved CKII–PEST region of E7 and its phosphorylation modulate the binding kinetics without modifying the interaction mechanism. The CKII–PEST region stabilizes the complex between the LxCxE motif and RbAB (Fig. 3 and Table 1) through electrostatic interactions that speed up association, further contributing to orienting the motif. This is in accordance with previous results showing that this region contributes to RbAB binding,[38] although the magnitude of the electrostatic effect was lower than expected given the high proportion of charged residues found in this region (Fig. 1b and Table 2). The presence of a stretch of negatively charged residues following the LxCxE motif also increases RbAB binding affinity in the HDAC protein,[11] suggesting that electrostatic interactions play a role in binding of both cellular and viral Rb targets. Phosphorylation contributes electrostatic interactions (Fig. 3), similar to the CKII–PEST region. However, the stabilizing contribution of the CKII–PEST region is 90% present in the transition state for the association reaction, while the stabilizing contribution of phosphorylation is only 50% present in the transition state for the association reaction. This suggests that the interactions made by the CKII–PEST region and the phosphate groups may be of different nature, although they are both negatively charged. We speculate that the CKII–PEST region contributes long-range electrostatic interactions, which have few conformational restrictions and can thus form early in the association route. In turn, the phosphate groups would establish both long-range interactions early in the association route and short-range, conformationally restricted contacts with the RbAB domain that can only form late in the association route. The CKII–PEST region is present in HPVE7, AdE1A and SV40-LT and modulates their function.[58,70,71] In contrast, in cellular targets, the acidic region can be present (HDAC, RBP1 and RIZ) or absent (CtIP, CyclinD and BRG1/BRM), and only one-third of the targets present a phosphorylation site. This suggests that while the LxCxE motif provides a high-affinity anchoring site for both viral and cellular targets, the CKII–PEST region contributes to fine-tuning of the RbAB interaction dynamics in favor of viral proteins. The intrinsically disordered nature of the E7N domain allows for presentation of these linear motifs (LxCxE and CKII–PEST) for recognition by protein targets such as Rb.[31,36]

The dynamics of the complexes formed by Rb will dictate ligand competition between Rb targets. E7 binds to RbAB with an on-rate of 1.5 10^{7} M^{-1} s^{-1}, 1 order of magnitude faster than the on-rate of the E2F-1 transactivation domain, measured by surface plasmon resonance[10] to be $k_{on}=1$ 10^{6} M^{-1} s^{-1}. A faster association rate would provide E7 with an advantage for displacement of E2F because E7-induced Rb degradation will turn this interaction into an "irreversible" process, further decreasing the number of Rb molecules available for interaction with E2F. On the other hand, differences in the half-life of the complexes may also be relevant to E7 function. For example, NMR titrations showed that differences in affinity between LxCxE peptides from HDAC1 and HPV16 E7 were reflected by changes in the exchange dynamics and, therefore, the k_{off} of the complexes, suggesting that E7 may easily displace preformed complexes of cellular targets such as HDAC from the LxCxE binding site.[11] Rather small differences in Rb binding strength are also related to the variable transforming potential of prototypical high-risk HPV16 and HPV18 and low-risk HPV11 E7 proteins.[42,61] Figure 4 shows that these differences also lie on the dissociation rates, leading us to suggest that changes in ligand exchange dynamics may render low-risk HPV11 E7 proteins less potent in displacing cellular Rb complexes, contributing to the differences in the transforming potential of these proteins.[42] HPV16 E7 presents a negatively charged aspartate at position 21 of its LxCxE motif (Fig. 1b). Interestingly, replacement for a positively charged arginine in HDAC1 and for a neutral glycine in HPV11 E7 accounts for the differences in affinity and exchange dynamics between these proteins.[11,61]

The E7:RbAB binding reaction features two characteristics that are common to many naturally

occurring protein–protein interactions yet have been hardly explored by biophysical or kinetic experiments to date. First, the complex has multiple sites of interaction with different binding strengths, namely, the high-affinity LxCxE motif and its modulators and the low-affinity E7C domain. This is shared with many other eukaryotic proteins, where multiple interacting modular domains are often present.[72,73] Second, while the RbAB domain displays a compact fold,[20] E7 shows remarkable structural plasticity, particularly in the E7N domain[31] (Fig. 1a). This plasticity suggests two potential consequences: on one hand, the ability to adopt many different conformations may provide with multiple efficient binding routes; on the other, the transition from a flexible free E7 to a more rigid bound form may create kinetic bottlenecks in this coupled folding–binding process.[74,75]

Our results show that the presence of multiple anchoring sites and coupled folding and binding lead to considerable kinetic complexity in the association of full-length E7 to RbAB (Figs. 5 and 6). At least two intermediates are significantly populated during binding, indicative of a frustrated energy landscape with several deep wells.[76] Only a fraction of free E7 molecules are competent for binding. Since the binding kinetics of the E7N domain are two state, we suggest that the E7 pre-equilibrium reaction stems from a slow isomerization in the E7C domain and/or from yet unknown E7N–E7C inter-domain interactions that preclude fast association. Association starts by an electrostatically steered docking of the charged LxCxE motif, showing that this region not only is the main determinant of the binding thermodynamics[36] but also provides the fastest route for complex formation. The last step of the reaction is a slow unimolecular rearrangement of the E7:RbAB complex. We propose that, in this rate-limiting reaction, the RbAB domain remains compact[20,77] and that, within the flexible E7, the LxCxE motif remains docked and other parts of the molecule undergo a conformational rearrangement. This mechanism resembles that described for the coupled folding and binding of unstructured pKID to the KIX domain, where an on-pathway partially folded intermediate was also identified.[78] In this system, disorder within pKID was also shown to optimize the binding kinetics.[79] Interestingly, whereas the pKID–KIX encounter complex was mainly stabilized by hydrophobic contacts,[78] the E7:RbAB encounter complex is stabilized by electrostatic interactions. Recent studies have shown that multiple anchoring sites and intrinsic disorder within adenovirus E1A also contribute to the formation of ternary complexes that compete effectively with cellular interactions.[22]

The salt dependence of the E7:RbAB interaction is remarkably complex. Electrostatic interactions favor complex formation for both the E7N domain and the full-length protein (Fig. 7a), with the main contributor to the electrostatic component within the E7N domain being the LxCxE module. However, the salt dependence is higher for the E7N domain (Table 2). We can interpret this result by assuming that the electrostatic interactions formed by the $E7_{16–40}$ fragment upon binding are the same in isolation and within the context of full-length E7. In this case, we can dissect the salt dependence of the E7:RbAB complex into additive contributions from the N-terminal and C-terminal domains of E7, and $\Gamma^{EQ}{}_{NaCl}$ (E7) = $\Gamma^{EQ}{}_{NaCl}$ ($E7_{16–40}$) + $\Gamma^{EQ}{}_{NaCl}$ (E7C). If this is correct, $\Gamma^{EQ}{}_{NaCl}$ (E7C) = −1.16 + 1.82 = 0.66. In other words, the electrostatic interactions formed by the E7C domain upon binding are unfavorable. This may contribute to the observation that the binding free energy for the full-length E7 protein is less than the sum of the binding free energies of the isolated E7N and E7C domains.[36] The association kinetics reveal additional intricacies (Fig. 7): whereas the pre-equilibrium reaction and the formation of the intermediate complex show little salt dependence at equilibrium, all the corresponding forward and reverse reactions are strongly slowed down by salt. Thus, for these two conformational transitions, electrostatic interactions are more favorable in the TSEs than in the ground states. The following speculative scenario can explain this observation. In the ground states, charges are held in an unfavorable configuration by the rest of the molecule. This electrostatic frustration is released to some extent in the TSE via partial "cracking" of the structure,[76,80] leading to stabilization of the TSE relative to both ground states of the reaction. Altogether, probing the energy landscape for E7:RbAB association by salt further supports the presence of a significant amount of frustration in this reaction.

The present study allows us to present an overall picture of the E7:RbAB interaction, which reveals important features concerning the role of the LxCxE motif and of secondary interactions sites present in E7 on the binding kinetics. As in equilibrium, the LxCxE motif within the intrinsically disordered E7N domain plays a crucial role by acting as a high-affinity anchor around of which the rest of the complex interface forms. Binding of the minimal LxCxE regulatory module shows simple yet highly optimized kinetics,[79] with enough affinity and a half-life to allow for competition with cellular proteins at low expression levels typical of early stages of natural infections. The downstream acidic stretch, reversible phosphorylation and other proximal charges may shape this competition in an HPV-type-dependent manner. The multiple binding sites within the flexible E7 lead to complex kinetics and the population of frustrated species. We present a first approach to the study of the E7:Rb interaction mechanism. Future efforts that extend the present

study including other Rb domains and competition studies should help elucidate the contribution from interactions between the E7C and the RbC domains and uncover the mechanisms for E2F displacement. The complexity observed in E7:Rb binding kinetics is likely involved in fine-tuning the displacement of cellular Rb targets that also present multiple interaction sites and will determine the ensuing transient and long-term effects on the Rb interaction network upon E7 over-expression.

Materials and Methods

Protein expression and purification

The human RbAB domain (residues 372–787) and the HPV16 E7 protein (residues 1–98) were expressed and purified as previously described.[33,36] Briefly, the RbAB domain was cloned in the pRSET-A vector, expressed as a His-tagged fusion protein and purified through metal-affinity chromatography followed by ion-exchange and size-exclusion chromatographies. The HPV16 E7 protein was cloned in the pMalE vector, expressed as a maltose binding protein fusion protein and purified through an amylose resin followed by ion-exchange and size-exclusion chromatographies preceded by a refolding step that was included in order to obtain a conformationally homogeneous sample. The RbAB domain was obtained as a monomer as determined by its gel-filtration profile and static light-scattering measurements, and the E7 protein was obtained as a homogeneous dimer with 1 mol of bound zinc per protein monomer. Protein purity was >95% as judged by SDS/PAGE, and protein identity was confirmed by Western blots and by matrix-assisted laser desorption/ionization time-of-flight mass spectrometry (Bruker Daltonics, Billerica, MA, USA). Protein concentration was determined by the Bradford method using bovine serum albumin as a standard or by UV spectroscopy using reported extinction coefficients for tyrosine and tryptophan.[81]

Peptide synthesis and labeling

The synthesis and labeling of the E7 peptides used in this work have been previously described in detail.[36] Briefly, peptides were synthesized by F-moc chemistry (W. M. Keck Facility, Yale University, New Haven, CT). FITC labeling at the free N-terminus was carried out in 100 mM sodium carbonate buffer, pH 8.0, for 2 h at room temperature, and labeled peptides were separated from free FITC by a PD-10 column (GE Healthcare, Uppsala, Sweden) followed by size-exclusion chromatography or reverse-phase HPLC. The purity of all preparations was judged by matrix-assisted laser desorption/ionization time-of-flight spectroscopy. Peptides were quantified by UV absorbance at 220 nm in HCl, and the FITC concentration was determined at pH 7.0 and 495 nm using a molar extinction coefficient of 75,000 M^{-1} cm^{-1}.[82] The synthetic peptides used in this study are shown in Fig. 1b.

Chemicals and solutions

Unless stated otherwise, all measurements were performed in 20 mM sodium phosphate buffer (pH 7.0), 200 mM NaCl, 2 mM DTT and 0.1% Tween 20 at 20 ± 0.1 °C. All chemical reagents were of analytical grade (purchased from Sigma-Aldrich or ICN Biomedicals), and all solutions were prepared with distilled and deionized (Milli-Q plus) water and filtered through 0.22-μm membranes prior to use.

Kinetic measurements

Kinetic measurements were performed using an SX18MV stopped-flow apparatus (Applied Photophysics, Leatherhead, UK) except when stated otherwise. All concentrations reported are those of the measurement cell, which resulted from mixing equal volumes of protein solutions from each stopped-flow syringe. The association and dissociation reactions were monitored by following the change in fluorescence intensity or fluorescence anisotropy of the FITC moiety coupled to the E7 peptides or the E7 protein. For FITC fluorescence measurements, the excitation monochromator was set to 495 nm with a 4.6-nm band-pass, and emission was collected through a 515-nm-cutoff filter (Schott, PA, USA). For FITC anisotropy measurements, two photomultiplier tube detectors were assembled in T-geometry, and vertically and horizontally polarized emissions were collected through 530-nm-cutoff filters. For reactions showing slow dissociation kinetics, measurements were performed in a fluorescence polarimeter (Aminco-Bowman) assembled in L-geometry using a 500-μl quartz cuvette and setting the excitation and emission wavelengths to 495 nm and 520 nm, respectively, with a 4- to 8-nm bandwidth.

Pseudo-first-order association kinetics

For the $E7_{16–31}$, $E7_{16–40}$ and $E7_{16–40PP}$ fragments and for the full-length E7 protein, association reactions were measured in pseudo-first-order regime with respect to RbAB by monitoring the change in FITC fluorescence intensity upon RbAB binding. FITC-peptide/protein concentration was held constant at 5 nM, and RbAB concentration was varied between 25 and 400 nM. Eight to ten time traces were averaged per measurement point.

Non-pseudo-first-order association kinetics

The association and dissociation between the HPV16, HPV11 and HPV18 E7N domains and RbAB were followed by the change in fluorescence anisotropy of the FITC moiety coupled to the peptides. Because of greater limitations in the signal-to-noise ratio of these measurements, the association traces were recorded at 200 nM FITC-E7N and at RbAB concentrations varying from 100 to 2000 nM. Eight to ten time traces were averaged per measurement point.

Dissociation kinetics

Dissociation traces were measured by displacing a stoichiometric complex of RbAB and FITC-labeled E7

peptide/protein at 25 nM concentration by adding a 25- to 50-fold excess of unlabeled E7 peptide/protein. For dissociation traces recorded in the fluorescence spectrometer, the change in fluorescence upon dissociation could be compared to the original fluorescence signal of the free peptide/protein, verifying the reversibility of the reaction. Five to ten kinetic traces were averaged per measurement.

Interrupted association experiments

Experiments were performed by first mixing equal volumes of RbAB protein and FITC-labeled $E7_{16–31}$ peptide at a final concentration of 50 nM RbAB and 10 nM FITC-$E7_{16–31}$. After a delay time ranging from 50 to 5000 ms, the dissociation kinetics were measured by mixing the complex with an excess amount (2.5 μM) of unlabeled $E7_{16–31}$ peptide.

Data analysis and fitting

Fitting was carried out using the Profit software (Quantumsoft, Zurich, Switzerland) to obtain parameters and their standard deviations.

Pseudo-first-order association traces

Averages of 5–10 kinetic traces containing at least 1000 measurement points for the HPV16 $E7_{16–31}$, $E7_{16–40}$ and $E7_{16–40PP}$ peptides at 5 nM FITC-peptide and at each RbAB concentration were fit to Eq. (1) to obtain the observed rate constant:

$$F(t) = F_0 + A \cdot e^{k_{obs}t} + c_1 t \quad (1)$$

where A is the amplitude and k_{obs} the observed rate constant. Signal drift was taken into account by a linear time-dependent term (c_1), and the initial fluorescence value was F_o. The k_{obs} values as a function of RbAB concentration were fit to Eq. (2) to obtain the microscopic association and dissociation rate constants for the reaction (k_{on} and k_{off}):

$$k_{obs} = k_{off} + k_{on} \times [RbAB] \quad (2)$$

Dissociation kinetics

Dissociation traces performed in excess of unlabeled ligand were fit to a mono-exponential function of the form [Eq. (1)] to obtain the k_{off} value.

Non-pseudo-first-order association traces

Under our measurement conditions, all association traces for E7N domains had mono-exponential kinetics. The dependence of the observed association rate constant (k_{obs}) on RbAB concentration was fit to Eq. (3), which describes the dependence of k_{obs} on the kinetic rate constants for bimolecular association processes under non-pseudo-first-order conditions,[83] and has been applied to describe protein/peptide interactions:[66,84]

$$k_{obs} = \sqrt{k_{on}^2(n - [RbAB])^2 + k_{off}^2 + 2k_{on}k_{off}(n + [RbAB])} \quad (3)$$

where k_{obs} is the observed rate constant at each RbAB concentration point and n is the fixed concentration of FITC-labeled peptide. This allowed for the determination of the values for k_{on} and k_{off}. Under pseudo-first-order conditions ($n \ll [RbAB]$), Eq. (3) breaks down to Eq. (2).

Complex association and dissociation kinetics

For the full-length E7 protein, association traces under pseudo-first-order conditions yielded complex kinetics that did not fit to a single-exponential function. These traces were fit to a combination of up to three exponential functions (with amplitudes A_n and rates k_n):

$$F(t) = A_1 \cdot e^{k_1 t} + A_2 \cdot e^{k_2 t} + A_3 \cdot e^{k_3 t} + c_1 \cdot t + c_2 \quad (4)$$

Signal drift was taken into account by a linear time-dependent term (c_1), and the initial fluorescence value was F_o.

Quantitative modeling of the E7:RbAB interaction

We considered the following linear four-state mechanism for the association between E7 and RbAB, described by Scheme 2.

Under pseudo-first-order conditions ($[Rb] = [Rb]_T$), this mechanism is described by differential Eqs. (6)–(9):

$$\frac{\partial[E7^*]}{\partial t} = -k_1[E7^*] + k_{-1}[E7] \quad (6)$$

$$\frac{\partial[E7]}{\partial t} = k_1[E7^*] - (k_2 Rb_T + k_{-1})[E7] + k_{-2}(Rb : E7) \quad (7)$$

$$\frac{\partial[(E7 : Rb)]}{\partial t} = k_2 Rb_T[E7] - (k_{-2} + k_3)[(Rb : E7)] + k_{-3}[[E7 : Rb]] \quad (8)$$

$$\frac{\partial[[E7 : Rb]]}{\partial t} = k_3[(Rb : E7)] - k_{-3}[[Rb : E7]] \quad (9)$$

where k_n and k_{-n} are the forward and reverse rate constants for the nth equilibrium, respectively, and the RbAB domain is denoted as Rb for simplicity. This system can be solved by matrix substitution methods and gives rise to the third-order characteristic polynomial:

$$\lambda^3 + C_1\lambda^2 + C_2\lambda + C_3 = 0 \quad (10)$$

where C_1, C_2 and C_3 are coefficients that depend on the microscopic rate constants and on Rb concentration (Supplementary Fig. 8). Solving this polynomial for λ yields the three nonzero eigenvalues that correspond to the three observed relaxation phases (Supplementary Fig. 8). We used this model

$$E7^* \underset{k_{-1}}{\overset{k_1}{\rightleftharpoons}} E7 + RbAB \underset{k_{-2}}{\overset{k_2}{\rightleftharpoons}} (E7{:}RbAB) \underset{k_{-3}}{\overset{k_3}{\rightleftharpoons}} [E7{:}RbAB]$$

Scheme 2. Kinetic association route for the [E7:RbAB] complex.

to perform a global fit of dependence of k_{obs1}, k_{obs2} and k_{obs3} on RbAB concentration at different [NaCl] concentrations, restricting the fit with the K_d value obtained by equilibrium titrations performed at each NaCl concentration tested. Quantitative modeling of the other two four-state mechanisms for the E7:Rb interaction discussed in the Results setion are also described in Supplementary Fig.8.

NaCl dependence of the equilibrium and kinetic rate constants

The dependence of the equilibrium and kinetic constants on NaCl concentration was assessed by performing experiments in reaction buffer [20 mM sodium phosphate (pH 7.0), 2 mM DTT and 0.1% Tween 20] supplemented with varying concentrations of NaCl ranging between 0.05 and 1 M. Equilibrium titrations were performed as previously described.[36] For the $E7_{16–31}$, $E7_{16–40}$ and $E7_{16–40PP}$ peptides and for the E7 protein, measurements were performed by following the change in fluorescence intensity of the FITC-labeled peptides/protein. Kinetic association traces were recorded in pseudo-first-order regime at 5 nM [FITC-E7 peptide/protein] and 50 nM [RbAB]. Kinetic dissociation traces were recorded as described above, by displacement of a 25-nM stoichiometric complex of labeled peptide/protein and RbAB with excess amounts (1.25 μM) of unlabeled peptide/protein. The k_{off} values were calculated directly from fitting the fluorescence dissociation traces to a mono-exponential function, and the k_{on} values were calculated from Eq. (2) using the k_{off} values determined independently at each NaCl concentration. For the HPV16, HPV18 and HPV11 E7N domains, measurements were performed by following the change in fluorescence anisotropy of the FITC-labeled peptides. Kinetic association traces were recorded under non-pseudo-first-order conditions at 200 nM [FITC-E7N] and 300 nM [RbAB] (HPV16 E7N) or 1 μM [RbAB] (HPV18 and HPV11 E7N). Kinetic dissociation traces were recorded by displacement of a 200-nM stoichiometric complex of labeled peptide and RbAB with an excess amount (8 μM) of unlabeled peptide. The k_{off} values were calculated directly from fitting the anisotropy dissociation traces to a mono-exponential function, and the k_{on} values were calculated from Eq. (3) using the k_{off} values determined independently at each NaCl concentration. Standard deviations for each kinetic constant were calculated by error propagation of the standard deviations of fitted parameters.

RbAB equilibrium titrations

Equilibrium titrations were performed in the same reaction buffer and temperature used for kinetic measurements by adding increasing amounts of RbAB domain to a cuvette containing a fixed concentration (5 nM) of FITC-labeled peptide. Measurements were performed after equilibration of the complex using a fluorescence polarimeter assembled in L-geometry, and fitting to a 1:1 association model was performed as previously described.[36] The K_d values reported in Table 1 were obtained by averaging the parameters obtained in four (HPV16 E7N) or five (HPV11 E7N and HPV18 E7N) independent experiments. For all interactions, stoichiometry was shown to be 1:1 by titrations performed at peptide concentrations 10 times greater than the determined K_d as detailed in Ref. 36. In order to assess the effect of NaCl on the $E7_{16–31}$:RbAB and the E7:RbAB interactions, we performed equilibrium titrations in reaction buffer containing varying amounts of NaCl.

Acknowledgements

L.B.C. currently holds a postdoctoral fellowship from Consejo Nacional de Investigaciones Científicas y Técnicas and was supported throughout the work by a José A. Estenssoro predoctoral fellowship from Fundación YPF. I.E.S. and G.d.P.-G. are career investigators from Consejo Nacional de Investigaciones Científicas y Técnicas. We thank M. Trevisan for helpful advice on quantitative modeling of the E7:Rb interaction.

Supplementary Data

Supplementary data to this article can be found online at doi:10.1016/j.jmb.2011.07.015

References

1. Chinnam, M. & Goodrich, D. W. (2011). RB1, development, and cancer. *Curr. Top. Dev. Biol.* **94**, 129–169.
2. Longworth, M. S. & Dyson, N. J. (2010). pRb, a local chromatin organizer with global possibilities. *Chromosoma*, **119**, 1–11.
3. van den Heuvel, S. & Dyson, N. J. (2008). Conserved functions of the pRB and E2F families. *Nat. Rev., Mol. Cell Biol.* **9**, 713–724.
4. Burkhart, D. L. & Sage, J. (2008). Cellular mechanisms of tumour suppression by the retinoblastoma gene. *Nat. Rev., Cancer*, **8**, 671–682.
5. Howley, P. M. & Livingston, D. M. (2009). Small DNA tumor viruses: large contributors to biomedical sciences. *Virology*, **384**, 256–259.
6. Morris, E. J. & Dyson, N. J. (2001). Retinoblastoma protein partners. *Adv. Cancer Res.* **82**, 1–54.
7. DeGregori, J. (2004). The Rb network. *J. Cell Sci.* **117**, 3411–3413.
8. Isaac, C. E., Francis, S. M., Martens, A. L., Julian, L. M., Seifried, L. A., Erdmann, N. *et al.* (2006). The retinoblastoma protein regulates pericentric heterochromatin. *Mol. Cell. Biol.* **26**, 3659–3671.
9. Xiao, B., Spencer, J., Clements, A., Ali-Khan, N., Mittnacht, S., Broceno, C. *et al.* (2003). Crystal structure of the retinoblastoma tumor suppressor protein bound to E2F and the molecular basis of its regulation. *Proc. Natl Acad. Sci. USA*, **100**, 2363–2368.
10. Lee, C., Chang, J. H., Lee, H. S. & Cho, Y. (2002). Structural basis for the recognition of the E2F transactivation domain by the retinoblastoma tumor suppressor. *Genes Dev.* **16**, 3199–3212.

11. Singh, M., Krajewski, M., Mikolajka, A. & Holak, T. A. (2005). Molecular determinants for the complex formation between the retinoblastoma protein and LXCXE sequences. *J. Biol. Chem.* **280**, 37868–37876.
12. Dick, F. A. (2007). Structure–function analysis of the retinoblastoma tumor suppressor protein—is the whole a sum of its parts? *Cell Div.* **2**, 26.
13. Burke, J. R., Deshong, A. J., Pelton, J. G. & Rubin, S. M. (2010). Phosphorylation-induced conformational changes in the retinoblastoma protein inhibit E2F transactivation domain binding. *J. Biol. Chem.* **285**, 16286–16293.
14. Rubin, S. M., Gall, A. L., Zheng, N. & Pavletich, N. P. (2005). Structure of the Rb C-terminal domain bound to E2F1-DP1: a mechanism for phosphorylation-induced E2F release. *Cell*, **123**, 1093–1106.
15. de Souza, R. F., Iyer, L. M. & Aravind, L. (2009). Diversity and evolution of chromatin proteins encoded by DNA viruses. *Biochim. Biophys. Acta*, **1799**, 302–318.
16. Kehn, K., Fuente Cde, L., Strouss, K., Berro, R., Jiang, H., Brady, J. *et al.* (2005). The HTLV-I Tax oncoprotein targets the retinoblastoma protein for proteasomal degradation. *Oncogene*, **24**, 525–540.
17. Munakata, T., Nakamura, M., Liang, Y., Li, K. & Lemon, S. M. (2005). Down-regulation of the retinoblastoma tumor suppressor by the hepatitis C virus NS5B RNA-dependent RNA polymerase. *Proc. Natl Acad. Sci. USA*, **102**, 18159–18164.
18. Forng, R. Y. & Atreya, C. D. (1999). Mutations in the retinoblastoma protein-binding LXCXE motif of rubella virus putative replicase affect virus replication. *J. Gen. Virol.* **80**, 327–332.
19. Davey, N. E., Trave, G. & Gibson, T. J. (2011). How viruses hijack cell regulation. *Trends Biochem. Sci.* **36**, 159–169.
20. Lee, J. O., Russo, A. A. & Pavletich, N. P. (1998). Structure of the retinoblastoma tumour-suppressor pocket domain bound to a peptide from HPV E7. *Nature*, **391**, 859–865.
21. Kim, H. Y., Ahn, B. Y. & Cho, Y. (2001). Structural basis for the inactivation of retinoblastoma tumor suppressor by SV40 large T antigen. *EMBO J.* **20**, 295–304.
22. Ferreon, J. C., Martinez-Yamout, M. A., Dyson, H. J. & Wright, P. E. (2009). Structural basis for subversion of cellular control mechanisms by the adenoviral E1A oncoprotein. *Proc. Natl Acad. Sci. USA*, **106**, 13260–13265.
23. Liu, X. & Marmorstein, R. (2007). Structure of the retinoblastoma protein bound to adenovirus E1A reveals the molecular basis for viral oncoprotein inactivation of a tumor suppressor. *Genes Dev.* **21**, 2711–2716.
24. Dyson, N., Guida, P., McCall, C. & Harlow, E. (1992). Adenovirus E1A makes two distinct contacts with the retinoblastoma protein. *J. Virol.* **66**, 4606–4611.
25. Patrick, D. R., Oliff, A. & Heimbrook, D. C. (1994). Identification of a novel retinoblastoma gene product binding site on human papillomavirus type 16 E7 protein. *J. Biol. Chem.* **269**, 6842–6850.
26. Block, C., Janknecht, R., Herrmann, C., Nassar, N. & Wittinghofer, A. (1996). Quantitative structure–activity analysis correlating Ras/Raf interaction *in vitro* to Raf activation *in vivo*. *Nat. Struct. Biol.* **3**, 244–251.
27. Kiel, C. & Serrano, L. (2009). Cell type-specific importance of ras–c-raf complex association rate constants for MAPK signaling. *Sci. Signal.* **2**, ra38.
28. Schreiber, G. (2002). Kinetic studies of protein–protein interactions. *Curr. Opin. Struct. Biol.* **12**, 41–47.
29. Phelps, W. C., Yee, C. L., Munger, K. & Howley, P. M. (1988). The human papillomavirus type 16 E7 gene encodes transactivation and transformation functions similar to those of adenovirus E1A. *Cell*, **53**, 539–547.
30. Banerjee, N. S., Genovese, N. J., Noya, F., Chien, W. M., Broker, T. R. & Chow, L. T. (2006). Conditionally activated E7 proteins of high-risk and low-risk human papillomaviruses induce S phase in postmitotic, differentiated human keratinocytes. *J. Virol.* **80**, 6517–6524.
31. Garcia-Alai, M. M., Alonso, L. G. & de Prat-Gay, G. (2007). The N-terminal module of HPV16 E7 is an intrinsically disordered domain that confers conformational and recognition plasticity to the oncoprotein. *Biochemistry*, **46**, 10405–10412.
32. Uversky, V. N., Roman, A., Oldfield, C. J. & Dunker, A. K. (2006). Protein intrinsic disorder and human papillomaviruses: increased amount of disorder in E6 and E7 oncoproteins from high risk HPVs. *J. Proteome Res.* **5**, 1829–1842.
33. Alonso, L. G., Garcia-Alai, M. M., Nadra, A. D., Lapena, A. N., Almeida, F. L., Gualfetti, P. & Prat-Gay, G. D. (2002). High-risk (HPV16) human papillomavirus E7 oncoprotein is highly stable and extended, with conformational transitions that could explain its multiple cellular binding partners. *Biochemistry*, **41**, 10510–10518.
34. Liu, X., Clements, A., Zhao, K. & Marmorstein, R. (2006). Structure of the human papillomavirus E7 oncoprotein and its mechanism for inactivation of the retinoblastoma tumor suppressor. *J. Biol. Chem.* **281**, 578–586.
35. Ohlenschlager, O., Seiboth, T., Zengerling, H., Briese, L., Marchanka, A., Ramachandran, R. *et al.* (2006). Solution structure of the partially folded high-risk human papilloma virus 45 oncoprotein E7. *Oncogene*, **25**, 5953–5959.
36. Chemes, L. B., Sanchez, I. E., Smal, C. & de Prat-Gay, G. (2010). Targeting mechanism of the retinoblastoma tumor suppressor by a prototypical viral oncoprotein. Structural modularity, intrinsic disorder and phosphorylation of human papillomavirus E7. *FEBS J.* **277**, 973–988.
37. Rechsteiner, M. & Rogers, S. W. (1996). PEST sequences and regulation by proteolysis. *Trends Biochem. Sci.* **21**, 267–271.
38. Dick, F. A. & Dyson, N. J. (2002). Three regions of the pRB pocket domain affect its inactivation by human papillomavirus E7 proteins. *J. Virol.* **76**, 6224–6234.
39. Chan, H. M., Smith, L. & La Thangue, N. B. (2001). Role of LXCXE motif-dependent interactions in the activity of the retinoblastoma protein. *Oncogene*, **20**, 6152–6163.
40. Munger, K., Yee, C. L., Phelps, W. C., Pietenpol, J. A., Moses, H. L. & Howley, P. M. (1991). Biochemical and biological differences between E7 oncoproteins of the high- and low-risk human papillomavirus types are determined by amino-terminal sequences. *J. Virol.* **65**, 3943–3948.

41. Huang, P. S., Patrick, D. R., Edwards, G., Goodhart, P. J., Huber, H. E., Miles, L. *et al.* (1993). Protein domains governing interactions between E2F, the retinoblastoma gene product, and human papillomavirus type 16 E7 protein. *Mol. Cell. Biol.* **13**, 953–960.
42. Heck, D. V., Yee, C. L., Howley, P. M. & Munger, K. (1992). Efficiency of binding the retinoblastoma protein correlates with the transforming capacity of the E7 oncoproteins of the human papillomaviruses. *Proc. Natl Acad. Sci. USA*, **89**, 4442–4446.
43. Xue, B., Williams, R. W., Oldfield, C. J., Goh, G. K., Dunker, A. K. & Uversky, V. N. (2010). Viral disorder or disordered viruses: do viral proteins possess unique features? *Protein Pept. Lett.* **17**, 932–951.
44. Chemes, L. B., Sánchez, I.E., Alonso, L.G. & de Prat-Gay, G. (2011). Intrinsic Disorder in the human papillomavirus E7 protein. In *Flexible Viruses: Structural Disorder within Viral Proteins* (Longhi, S., Uversky, V.N., ed.), pp. in press. John Wiley and Sons.
45. Shoemaker, B. A., Portman, J. J. & Wolynes, P. G. (2000). Speeding molecular recognition by using the folding funnel: the fly-casting mechanism. *Proc. Natl Acad. Sci. USA*, **97**, 8868–8873.
46. Helt, A. M. & Galloway, D. A. (2003). Mechanisms by which DNA tumor virus oncoproteins target the Rb family of pocket proteins. *Carcinogenesis*, **24**, 159–169.
47. Magnaghi-Jaulin, L., Groisman, R., Naguibneva, I., Robin, P., Lorain, S., Le Villain, J. P. *et al.* (1998). Retinoblastoma protein represses transcription by recruiting a histone deacetylase. *Nature*, **391**, 601–605.
48. Stokes, P. H., Thompson, L. S., Marianayagam, N. J. & Matthews, J. M. (2007). Dimerization of CtIP may stabilize *in vivo* interactions with the Retinoblastoma-pocket domain. *Biochem. Biophys. Res. Commun.* **354**, 197–202.
49. Dick, F. A., Sailhamer, E. & Dyson, N. J. (2000). Mutagenesis of the pRB pocket reveals that cell cycle arrest functions are separable from binding to viral oncoproteins. *Mol. Cell. Biol.* **20**, 3715–3727.
50. MacLellan, W. R., Xiao, G., Abdellatif, M. & Schneider, M. D. (2000). A novel Rb- and p300-binding protein inhibits transactivation by MyoD. *Mol. Cell. Biol.* **20**, 8903–8915.
51. Miyake, S., Sellers, W. R., Safran, M., Li, X., Zhao, W., Grossman, S. R. *et al.* (2000). Cells degrade a novel inhibitor of differentiation with E1A-like properties upon exiting the cell cycle. *Mol. Cell. Biol.* **20**, 8889–8902.
52. Joerger, A. C. & Fersht, A. R. (2008). Structural biology of the tumor suppressor p53. *Annu. Rev. Biochem.* **77**, 557–582.
53. Clements, A., Johnston, K., Mazzarelli, J. M., Ricciardi, R. P. & Marmorstein, R. (2000). Oligomerization properties of the viral oncoproteins adenovirus E1A and human papillomavirus E7 and their complexes with the retinoblastoma protein. *Biochemistry*, **39**, 16033–16045.
54. Sheinerman, F. B., Norel, R. & Honig, B. (2000). Electrostatic aspects of protein–protein interactions. *Curr. Opin. Struct. Biol.* **10**, 153–159.
55. Vindigni, A., White, C. E., Komives, E. A. & Di Cera, E. (1997). Energetics of thrombin–thrombomodulin interaction. *Biochemistry*, **36**, 6674–6681.
56. Grucza, R. A., Bradshaw, J. M., Mitaxov, V. & Waksman, G. (2000). Role of electrostatic interactions in SH2 domain recognition: salt-dependence of tyrosyl-phosphorylated peptide binding to the tandem SH2 domain of the Syk kinase and the single SH2 domain of the Src kinase. *Biochemistry*, **39**, 10072–10081.
57. Fersht, A. R., Matouschek, A. & Serrano, L. (1992). The folding of an enzyme. I. Theory of protein engineering analysis of stability and pathway of protein folding. *J. Mol. Biol.* **224**, 771–782.
58. Chien, W. M., Parker, J. N., Schmidt-Grimminger, D. C., Broker, T. R. & Chow, L. T. (2000). Casein kinase II phosphorylation of the human papillomavirus-18 E7 protein is critical for promoting S-phase entry. *Cell Growth Differ.* **11**, 425–435.
59. Phelps, W. C., Munger, K., Yee, C. L., Barnes, J. A. & Howley, P. M. (1992). Structure–function analysis of the human papillomavirus type 16 E7 oncoprotein. *J. Virol.* **66**, 2418–2427.
60. Genovese, N. J., Banerjee, N. S., Broker, T. R. & Chow, L. T. (2008). Casein kinase II motif-dependent phosphorylation of human papillomavirus E7 protein promotes p130 degradation and S-phase induction in differentiated human keratinocytes. *J. Virol.* **82**, 4862–4873.
61. Munger, K., Werness, B. A., Dyson, N., Phelps, W. C., Harlow, E. & Howley, P. M. (1989). Complex formation of human papillomavirus E7 proteins with the retinoblastoma tumor suppressor gene product. *EMBO J.* **8**, 4099–4105.
62. Hassler, M., Singh, S., Yue, W. W., Luczynski, M., Lakbir, R., Sanchez-Sanchez, F. *et al.* (2007). Crystal structure of the retinoblastoma protein N domain provides insight into tumor suppression, ligand interaction, and holoprotein architecture. *Mol. Cell*, **28**, 371–385.
63. Schreiber, G. & Fersht, A. R. (1993). Interaction of barnase with its polypeptide inhibitor barstar studied by protein engineering. *Biochemistry*, **32**, 5145–5150.
64. Myles, T., Le Bonniec, B. F., Betz, A. & Stone, S. R. (2001). Electrostatic steering and ionic tethering in the formation of thrombin–hirudin complexes: the role of the thrombin anion-binding exosite-I. *Biochemistry*, **40**, 4972–4979.
65. Kiel, C., Selzer, T., Shaul, Y., Schreiber, G. & Herrmann, C. (2004). Electrostatically optimized Ras-binding Ral guanine dissociation stimulator mutants increase the rate of association by stabilizing the encounter complex. *Proc. Natl Acad. Sci. USA*, **101**, 9223–9228.
66. Gianni, S., Engstrom, A., Larsson, M., Calosci, N., Malatesta, F., Eklund, L. *et al.* (2005). The kinetics of PDZ domain–ligand interactions and implications for the binding mechanism. *J. Biol. Chem.* **280**, 34805–34812.
67. Stewart, R. C. & Van Bruggen, R. (2004). Association and dissociation kinetics for CheY interacting with the P2 domain of CheA. *J. Mol. Biol.* **336**, 287–301.
68. Zhang, Y., Wavreille, A. S., Kunys, A. R. & Pei, D. (2009). The SH2 domains of inositol polyphosphate 5-phosphatases SHIP1 and SHIP2 have similar ligand specificity but different binding kinetics. *Biochemistry*, **48**, 11075–11083.

69. Radic, Z., Kirchhoff, P. D., Quinn, D. M., McCammon, J. A. & Taylor, P. (1997). Electrostatic influence on the kinetics of ligand binding to acetylcholinesterase. Distinctions between active center ligands and fasciculin. *J. Biol. Chem.* **272**, 23265–23277.
70. Rihs, H. P., Jans, D. A., Fan, H. & Peters, R. (1991). The rate of nuclear cytoplasmic protein transport is determined by the casein kinase II site flanking the nuclear localization sequence of the SV40 T-antigen. *EMBO J.* **10**, 633–639.
71. Whalen, S. G., Marcellus, R. C., Barbeau, D. & Branton, P. E. (1996). Importance of the Ser-132 phosphorylation site in cell transformation and apoptosis induced by the adenovirus type 5 E1A protein. *J. Virol.* **70**, 5373–5383.
72. Grove, T. Z., Cortajarena, A. L. & Regan, L. (2008). Ligand binding by repeat proteins: natural and designed. *Curr. Opin. Struct. Biol.* **18**, 507–515.
73. Remenyi, A., Good, M. C. & Lim, W. A. (2006). Docking interactions in protein kinase and phosphatase networks. *Curr. Opin. Struct. Biol.* **16**, 676–685.
74. Mittag, T., Kay, L. E. & Forman-Kay, J. D. (2009). Protein dynamics and conformational disorder in molecular recognition. *J. Mol. Recognit.* **23**, 105–116.
75. Uversky, V. N. (2010). Multitude of binding modes attainable by intrinsically disordered proteins: a portrait gallery of disorder-based complexes. *Chem. Soc. Rev.* **40**, 1623–1634.
76. Ferreiro, D. U., Hegler, J. A., Komives, E. A. & Wolynes, P. G. (2011). On the role of frustration in the energy landscapes of allosteric proteins. *Proc. Natl Acad. Sci. USA*, **108**, 3499–3503.
77. Balog, E. R. M., Burke, J. R., Hura, G. L. & Rubin, S. M. (2011). Crystal structure of the unliganded retinoblastoma protein pocket domain. *Proteins: Struct., Funct., Bioinf.* **79**, 2010–2014.
78. Sugase, K., Dyson, H. J. & Wright, P. E. (2007). Mechanism of coupled folding and binding of an intrinsically disordered protein. *Nature*, **447**, 1021–1025.
79. Turjanski, A. G., Gutkind, J. S., Best, R. B. & Hummer, G. (2008). Binding-induced folding of a natively unstructured transcription factor. *PLoS Comput. Biol.* **4**, e1000060.
80. Whitford, P. C., Onuchic, J. N. & Wolynes, P. G. (2008). Energy landscape along an enzymatic reaction trajectory: hinges or cracks? *HFSP J.* **2**, 61–64.
81. Pace, C. N., Vajdos, F., Fee, L., Grimsley, G. & Gray, T. (1995). How to measure and predict the molar absorption coefficient of a protein. *Protein Sci.* **4**, 2411–2423.
82. Hermanson, G. T. (1996). *Bioconjugate Techniques.* Academic Press, San Diego, CA.
83. Malatesta, F. (2005). The study of bimolecular reactions under non-pseudo-first order conditions. *Biophys. Chem.* **116**, 251–256.
84. Chi, C. N., Bach, A., Engstrom, A., Wang, H., Stromgaard, K., Gianni, S. & Jemth, P. (2009). A sequential binding mechanism in a PDZ domain. *Biochemistry*, **48**, 7089–7097.